Nonperturbative treatment of multielectron processes in ion-molecule scattering: Application to He²⁺-H₂ collisions

Nicolas Sisourat,[1,2,*] Ingjald Pilskog,[1,3] and Alain Dubois[1,2]

[1]*Laboratoire de Chimie Physique - Matière et Rayonnement, UMR 7614, UPMC Université Paris 6, 11 rue Pierre et Marie Curie,*
F-75231 Paris Cedex 05, France
[2]*LCPMR, UMR 7614, CNRS, F-75005 Paris, France*
[3]*Department of Physics and Technology, University of Bergen, N-5007 Bergen, Norway*

We present a nonperturbative theory to describe multielectronic processes occurring in the course of collisions between an ion and a molecule. The approach is based on the expansion of the electronic scattering wave function onto asymptotic mono- or multicenter states with proper translational conditions and includes both static and dynamical electronic correlations. Therefore, it has a wide application range around intermediate impact velocities $v \approx v_e$, where v_e is the averaged electron velocity in the initial state. As a first application, we report results on single- and double-electron capture processes in He²⁺-H₂ collisions for impact energies ranging from 0.01 to 25 keV/u. Special emphasis on the prediction of cross sections for double-electron capture into doubly excited states of helium is addressed.

I. INTRODUCTION

The study of ion-molecule collisions and the detailed knowledge of the cross sections for the various electronic processes occurring in such events present a great interest in various domains such as astrophysics [1], plasma (e.g., fusion plasma [2]) physics, and in the medical sciences; for example, hadrontherapy [3,4] in which the ions are advantageous with respect to photons because hadrons allow better control of the dose distribution. It is also of fundamental importance since theoretical investigations, supported or motivated by experimental research, pave the long way for better understanding and modeling of dynamical many-body quantum systems. Indeed, even with present-day supercomputers, it is still not possible to evaluate routinely cross sections of electronic processes for impact energies ranging from the molecular (reactive) regime to the perturbative regime. This is true especially for many-electron, polynuclei systems, but there are still many unsolved problems and disagreements for problems with one active electron (see, e.g., [5]).

Scattering systems involving ions, diatomic molecules and one- and two-electron bound-bound transitions provide benchmark systems to test new approaches and their computer implementations for further extension to larger molecular targets (e.g., H₂O). Among them doubly charged ions are optimal projectiles to avoid the further complexity of dealing with large many-folds for the description of the dominant processes so that the α-particle–dihydrogen-molecule collision is the unavoidable reference system: it is a true two-electron system involving partners whose structures are well known and provides therefore a probe for the study of multicenter effects and of the influence of correlation on electronic processes. It has therefore been thoroughly studied over the last four decades.

In the seventies and eighties the experimental investigations of the He²⁺-H₂ scattering system were focused on single-electron processes: let us mention, among others, the studies performed at high impact energies (above 300 keV/u) by Hvelplund and Andersen [6] for electron transfer, at lower energies (down to 5 keV/u) by Rudd and collaborators [7] for ionisation and electron transfer and the numerous studies of state-selective single-electron transfer (see, e.g., [8–10]). In more recent years double-electron processes, (e.g., double transfer or transfer ionisation) were addressed by several groups [11–17]. One of the important problems to elucidate was the dominance of single- versus double-transfer processes at low (keV) impact energies (cf. [12,14,17]).

Theoretically the study of single- and double-electron processes in ion-molecule collisions is not an easy task when taking into account the electronic correlation and the multicenter features of the target. This particular challenge has therefore been often bypassed by the *effective center* approximation [18], which describes the electronic degrees of freedom of a randomly oriented target. Except at very low energies where quantal calculations are unavoidable nonperturbative approaches refer to the semiclassical approximation and to a pure molecular picture of the $(N + 1)$-center scattering system (i.e., molecular orbital close-coupling methods, or MOCC), with inclusion of proper translational factors, as described in Delos [19]. (See, for example, the important and thorough theoretical developments proposed by the Madrid group, [20] and [21] for He²⁺-H₂ collisions, and by Kimura and collaborators [14,22]). Other parallel approaches have been developed, such as the *asymptotic theory* described recently in Khoma *et al.* [23], in which the coupling matrix elements are approximately evaluated using asymptotic conditions. The pending methods to the MOCC ones are the atomic orbital close-coupling (AOCC) treatments which are based on the expansion of the scattering wave function onto states of the isolated collision partners and are therefore more suitable for intermediate impact energies. They are the extension of the methods developed in ion-atom collisions [24] and so far are confined to (quasi-)one-electron ion-diatomic-molecular target systems [25]. An alternative method, the so-called basis

generator method, has been recently extended from atomic to molecular targets (cf. the work of Lüdde and collaborators [26] for water molecule targets). It should be mentioned that various approximated simple models to describe single capture (and ionisation) for high impact energies have been developed, such as, for example the classical trajectory Monte Carlo (CTMC) method [27,28] or scaling rules definitions [29].

The present work is devoted to the description of a non-perturbative semiclassical method which extends the AOCC approach [25,30] to two-active-electron ion-molecule collisions. The aim is to provide a reliable tool to calculate cross sections for dominant electronic processes at intermediate impact energies that require taking into account both static and dynamic electronic correlations (cf. the discussion in Ref. [31] for double-electron processes in ion-atom collisions) and the multicenter features of the target. Our second objective is the evaluation of cross sections for double-electron capture into autoionizing states in low- and intermediate-energy He^{2+}-H_2 collisions in order to predict further extensions to low impact velocities of the single-electron interferometric experiments proposed theoretically by Barrachina and Zitnik [32] and performed a few years later by Chesnel and collaborators [33].

The present paper is organized as follows: The first section describes in detail our theoretical treatment and the second section is devoted to the presentation of the specific model for the collision system under consideration and of the results stemming from intensive calculations: emphasis is on the description of the one- and two-electron transfer processes, at the level of total cross sections, in comparison with experimental and theoretical data, and differential semiclassical probabilities. The presentation of the specific cross sections of double-capture to autoionizing states is the object of the final part of the paper, with discussion of the feasibility of the experiments in the low-energy range for which little is known. After concluding remarks the paper ends with two appendices giving the details on (i) the method which has been developed to compute the various and complex matrix elements required in our theoretical model and (ii) the basis set which has been used in the calculations.

In the following atomic units are used, unless otherwise stated.

II. THE THEORETICAL APPROACH

To describe ion–diatomic-molecule collisions at intermediate impact velocities (i.e., when $v \approx v_e$, with v_e being the averaged electron velocity in the initial state), we use the well-established impact parameter semiclassical method [24,34]. In this energy range a theoretical treatment must couple the different open channels, including excitation, electron transfer, ionization, and all multielectronic combined processes. For example, in the next section we focus on the analysis of (pure) single transfer, transfer excitation, and double transfer, respectively,

$$P^{q+} + AB(0) \longrightarrow \begin{cases} P^{(q-1)+}(k) + AB^+(0) \\ P^{(q-1)+}(k) + AB^+(j) \\ P^{(q-2)+}(k') + AB^{2+}(0), \end{cases} \quad (1)$$

where $0\,(j,k,k')$ represents schematically the ground (excited) state of the collision partners. A nonperturbative quantum treatment for the electrons is therefore adopted while the projectile-target relative motion is described by classical straight-line, constant velocity trajectories.

The two-electron time-dependent Schrödinger equation (TDSE) (also called the *eikonal* equation) can then be written as

$$\left[H - i \left. \frac{\partial}{\partial t} \right|_{\vec{r}_1, \vec{r}_2} \right] \Psi(\vec{r}_1, \vec{r}_2, \vec{R}(t)) = 0, \quad (2)$$

with H being the electronic Hamiltonian

$$H = \sum_{i=1,2} \left[-\frac{1}{2}\nabla_i^2 + V_T(r_i) + V_P(|\vec{r}_i - \vec{R}(t)|) \right] + \frac{1}{|\vec{r}_1 - \vec{r}_2|}, \quad (3)$$

where the $\vec{r}_i$ are position vectors of the electrons with respect to the center of mass of the target and the relative projectile-target position $\vec{R}$ defines the trajectory; that is, $\vec{R}(t) = \vec{b} + \vec{v}t$ where b and v are the impact parameter and velocity, respectively (cf. Fig. 1). The term $V_T(r_i)$ [$V_P(|\vec{r}_i - \vec{R}(t)|)$] defines the effective electron-target [electron-projectile] core (AB^{2+} and P^{q+}, respectively) potential. Our approach is based on the rovibrational sudden approximation: the nuclei of the molecular target are frozen during the collisions stage (i.e., fixed $\vec{R}_{AB}$). This assumption is valid in the keV/u energy range since the electronic processes take place in a time range much shorter (subfemtosecond) than the vibrational motion of any molecule (>10 fs). The limit of this approximation will be discussed in the next section for the collision system He^{2+}-H_2. Note that, since in this approximation the core-core potential between the two nuclei A and B is constant, it only contributes through a common phase in the wave function and has thus been taken out from the Hamiltonian.
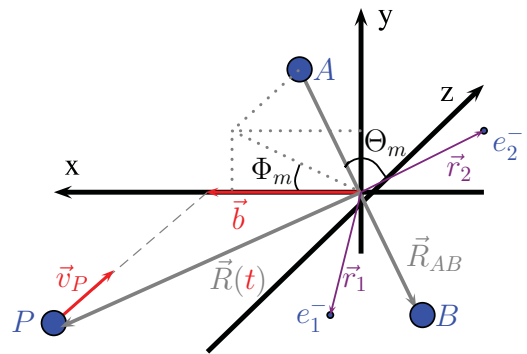

FIG. 1. (Color online) Collision geometry. The impact parameter $\vec{b}$ and the relative velocity $\vec{v}$ define the collision plane (xz) and the projectile (P) trajectory $\vec{R}(t)$ with respect to the molecular target represented by the two nuclei A and B, separated by internuclear vector $\vec{R}_{AB}$. The angles (Θ_m, Φ_m) define the molecular orientation with respect to $\vec{v}$ and $\vec{b}$.

The time-dependent Schrödinger equation is solved by expanding the wave function on a basis set of states of the isolated collision partners

$$
\begin{aligned}
\Psi(\vec{r}_1,\vec{r}_2,\vec{R}(t)) &= \sum_{i=1}^{N_{TT}} c_i^{TT}(t)\Phi_i^{TT}(\vec{r}_1,\vec{r}_2)e^{-iE_i^{TT}t} \\
&+ \sum_{j=1}^{N_{PP}} c_j^{PP}(t)\Phi_j^{PP}(\vec{r}_1,\vec{r}_2,\vec{R}(t))e^{-iE_j^{PP}t} \\
&+ \sum_{k=1}^{N_T}\sum_{l=1}^{N_P} c_{kl}^{TP}(t)\big[\phi_k^T(\vec{r}_1)\phi_l^P(\vec{r}_2,\vec{R}(t)) \\
&\pm \phi_k^T(\vec{r}_2)\phi_l^P(\vec{r}_1,\vec{R}(t))\big]e^{-i(E_k^T+E_l^P)t}, \quad (4)
\end{aligned}
$$

where the TT, PP, T, and P superscripts denote states (and corresponding energies) for which both electrons are respectively on the target (AB), on the projectile ($P^{(q-2)+}$) and on the target and projectile (AB^+ - $P^{(q-1)+}$). The two-electron states Φ are expressed as linear combinations of spin-adapted (singlet or triplet) products of Gaussian-type orbitals (GTOs) centered on A, B (target) or P (projectile):

$$
G_{\alpha_i,\ell,m}(\vec{r}) = Y_{\ell,m}(\hat{r})r^{\ell}e^{-\alpha_i r^2}, \quad (5)
$$

where the exponents α_i are selected by optimization (cf. Appendix B). The one-electron states ϕ are defined as linear combinations of GTOs centered on A, B, or P. The sign $+$ or $-$ in the last right-hand term of Eq. (4) is given by the spin symmetry of the states (singlet and triplet, respectively). For both electrons, the projectile states are augmented by plane-wave electron translation factors (ETFs) [35],

$$
\chi(\vec{r},t) = e^{i\vec{v}\cdot\vec{r}}e^{-i\frac{1}{2}v^2 t}, \quad (6)
$$

to ensure Galilean invariance of the results and to remove spurious dipolar coupling terms in the final equations to be solved [24].

The insertion of Eq. (4) into the TDSE results in a system of first-order coupled differential equations (CDEs), which are written in matrix form as

$$
i\,\underline{\underline{S}}(\vec{b},\vec{v},t)\frac{d}{dt}\underline{c}(t) = \underline{\underline{M}}(\vec{b},\vec{v},t)\underline{c}(t), \quad (7)
$$

where $\underline{c}$ is the column vector of the time-dependent expansion coefficients, c_i^{TT}, c_j^{PP} and c_{ij}^{TP} [Eq. (4)], $\underline{\underline{S}}$ and $\underline{\underline{M}}$ are the overlap and coupling matrices, respectively. It should be stressed that, within the present method, the electronic correlation, both static and dynamical as discussed in Ref. [31], is taken into account (cf. Appendix A). Moreover, the different channels described within the basis sets [Eq. (4)] are coupled during the dynamics; this is particularly important for multielectron processes (as double capture), which can proceed through several mechanisms. The CDEs are solved for a set of initial conditions (electronic state, velocity, impact parameter, and molecular target orientation at $t \to -\infty$) by a robust predictor-corrector time-step method developed by Shampine and Gordon [36]. The probability for a transition from the initial state Φ_I^{TT} to a final state Φ_F^{PP} (or Φ_F^{TT}, $\phi_f^T\phi_{f'}^P$) for an impact parameter $\vec{b}$, a fixed molecular orientation (Θ_m,Φ_m;

cf. Fig. 1), and a given projectile velocity $\vec{v}$, is given by the coefficient c_F^{PP} (respectively c_F^{TT} and $c_{ff'}^{TP}$) as follows:

$$
P_{I\to F}(v,\vec{b},R_{AB},\Theta_m,\Phi_m) = \lim_{t\to+\infty}\big|c_F^{PP}(t)\big|^2. \quad (8)
$$

The corresponding cross section for a given molecular orientation can be calculated from these probabilities as follows:

$$
\sigma_{IF}(v,R_{AB},\Theta_m) = \int d^2\vec{b}\, P_{I\to F}(v,\vec{b},R_{AB},\Theta_m,\Phi_m), \quad (9)
$$

where the dependence upon Φ_m disappears after integration over $\vec{b}$. In order to compare our predictions with experimental data which are generally performed with an isotropically oriented target sample, the cross sections in Eq. (9) must be averaged over the molecular orientations as

$$
\sigma_{IF}^{\text{tot}}(v,R_{AB}) = \frac{1}{2}\int_0^{\pi} d\Theta_m \sin\Theta_m \sigma_{IF}(v,R_{AB},\Theta_m). \quad (10)
$$

Since the computations of the probabilities are rather demanding, especially when involving numerous target orientation [Eqs. (9) and (10)], we have chosen to evaluate cross sections directly comparable with experimental data through an approximated averaging procedure using only three characteristic molecular orientations; namely $(\Theta_m,\Phi_m) = (0,0)$, $(0,\frac{\pi}{2})$, $(\frac{\pi}{2},\frac{\pi}{2})$:

$$
\begin{aligned}
\sigma_{IF}^{\text{tot}}(R_{AB}) = \frac{2\pi}{3}\bigg[&\varrho(v,R_{AB},0,0) + \varrho\left(v,R_{AB},0,\frac{\pi}{2}\right) \\
&+ \varrho\left(v,R_{AB},\frac{\pi}{2},\frac{\pi}{2}\right)\bigg],
\end{aligned} \quad (11)
$$

with

$$
\begin{aligned}
&\varrho(v,R_{AB},\Theta_m,\Phi_m) \\
&= \int_0^{+\infty} b P_{I\to F}(v,b,R_{AB},\Theta_m,\Phi_m)db. \quad (12)
\end{aligned}
$$

The approximation in Eqs. (11) and (12) has been proven to give good estimates of the total cross sections [5,20]. At this level, the cross sections depend upon the value of the molecular target internuclear distance R_{AB}. They should then be evaluated for different values of R_{AB} and averaged over the initial vibrational ground-state distribution. However, it has been shown that considering only the equilibrium distance value is sufficient to obtain accurate cross sections [5,30]. In the following we therefore consider only a molecular target fixed at the equilibrium geometry (the so-called Franck-Condon approximation; cf. [20]).

To conclude the presentation of this method, we summarize the various stages which should be performed to obtain the cross sections: (i) optimization of the GTO exponents [Eq. (5)] to describe the two-electron states of each of the isolated collision partners, (ii) diagonalization of the one- and two-electron Hamiltonians for each of the isolated partners using the set of GTOs obtained in the first stage, (iii) evaluation of the $\underline{\underline{S}}$ and $\underline{\underline{M}}$ matrix elements on a set of grid points along the projectile trajectories (cf. Appendix A), (iv) integration in time of Eq. (7) for a set of initial conditions, and (v) evaluation of total cross sections using Eqs. (11) and (12).

III. RESULTS AND DISCUSSION

In this section, after a presentation of the basis set used in the calculations, cross sections for single capture, transfer excitation, and double transfer are presented. A detailed comparison with a selection of experimental and theoretical data primes the discussion concerning the validity of the existing data and the possible reasons for remaining disagreements.

A. Model of He²⁺-H₂ collisions

To obtain probabilities and cross sections for the important processes occurring in He^{2+}-H_2 collisions in the low- to intermediate-energy range under consideration (i.e., from 10 eV/u to 25 keV/u), the method presented above is used for the Hamiltonian H defined as in Eq. (3) with

$$V_T(r_i) = -\frac{Z_A}{\left|\vec{r}_i - \frac{1}{2}\vec{R}_{AB}\right|} - \frac{Z_B}{\left|\vec{r}_i + \frac{1}{2}\vec{R}_{AB}\right|},$$

$$V_P(|\vec{r}_i - \vec{R}(t)|) = -\frac{Z_P}{|\vec{r}_i - \vec{R}(t)|}, \quad (13)$$

$Z_A = Z_B = 1$, $Z_P = 2$, and the internuclear distance R_{AB} of H_2 kept fixed at its equilibrium value (i.e., $R_{AB} = 1.4$ a.u.). The TDSE is solved with scattering states [Eq. (4)] developed onto several basis sets of various sizes and built from different sets of GTOs in order to check the accuracy and convergence of the results. The cross sections presented in the following are obtained by using a basis set composed of, besides numerous pseudostates, the well-identified lowest states of the different structures involved: 16 He states (6 bound states + 10 doubly excited states), 4 H_2 states, 10 He^+ states and 6 H_2^+ states combined into 60 antisymmetrized products of these states. Note that only singlet spin states are included in the basis set since the initial state, the ground state of H_2, is a singlet state and no spin transitions are allowed in the Hamiltonian. The two-electron states are obtained by optimization (genetic algorithm) of a set of 17 GTOs (12 for $\ell = 0$ and 5 for $\ell = 1$; cf. Table II in Appendix B) for He and 7 s-type GTOs on each center for H_2 (Table III in Appendix B). To decrease the number of matrix elements to be computed during the dynamical stage of the calculations, the one-electron He^+ and H_2^+ states are then obtained from the same respective

sets of GTOs. The quality of the states are estimated by comparing their energy to the experimental or exact values. The energy of the first bound states of the various atomic and molecular structures and of some autoionizing states of He included in the calculations are reported in Table I in which the good agreement with available data can be seen. The sets of GTOs presented above allow also the inclusion of 97 pseudostates (probability absorbers) to describe ionization channels. Note that this basis has been selected using two criteria: (i) large enough to describe accurately the important target and projectile states and (ii) still computationally tractable. Concerning the latter, the present basis is at the limit of our computer capacity and tests of convergence have been performed by comparing the present results with those from a slightly smaller basis set (reduced by 2 GTOs $\ell = 1$ on target and 1 GTO $\ell = 1$ on projectile) for which the He, He^+, H_2, and H_2^+ states are somewhat less accurately represented: the cross sections for single and double capture from these two sets agree with each other within 10%, except for the weak channels for which differences reach 25%. For double capture into doubly excited states the cross sections are rather small for the lowest considered energies (down to 0.8×10^{-18} cm², see below) and disagreement reaches 60% in this case only.

Finally, to solve Eq. (7) for a given set of initial conditions (impact velocity, impact parameter, and molecular orientation), the matrix elements were evaluated at 200 mesh points along the projectile trajectory, starting and ending when the centers are 60 a.u. apart. These two parameters, trajectory expansion and mesh points density, have been carefully tested through norm conservation and convergence of the transition probabilities. Finally, these latter have been evaluated for 20 impact parameters ranging from 0.5 to 10 a.u. to obtain converged cross sections.

B. Nondissociative and dissociative single-capture processes

As mentioned in the introduction, single- and double-electron capture processes in He^{2+}-H_2 collisions have been studied extensively, experimentally [6–14,17,37,38] as well as theoretically [14,21–23,39,40] and serious disagreements between the existing results remain. In Fig. 2 the cross sections for total single capture; namely, pure (nondissociative) single

TABLE I. Energies (a.u.) of the first bound and autoionizing (for He) states of the isolated collision partners computed with our GTO basis set compared to reference values from Ref. [44] (He⁺ and He), from Ref. [45] (He autoionizing states), and from Ref. [46] (H₂, H₂⁺). The values for H₂ and H₂⁺ are given for the internuclear distance $R_{AB} = 1.4$ a.u.

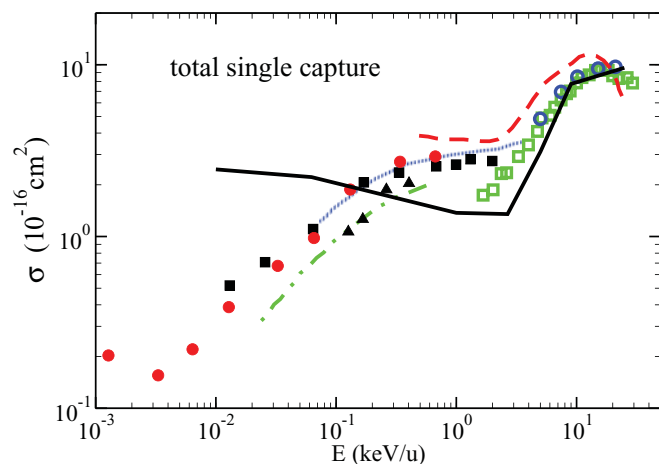| He⁺			He			H₂⁺			H₂		
State	E_{GTO}	E_{ref}	State	E_{GTO}	E_{ref}	State	E_{GTO}	E_{ref}	State	E_{GTO}	E_{ref}
$1s$	-2.000	-2.000	$^1S\ 1s^2$	-2.896	-2.904	σ	-1.274	-1.275	$^1\Sigma_g^+$	-1.868	-1.888
$2s$	-0.500	-0.500	$^1S\ 1s2s$	-2.144	-2.146	σ	-0.611	-0.613	$^1\Sigma_u^+$	-1.399	-1.420
$2p$	-0.499	-0.500	$^1P\ 1s2p$	-2.121	-2.124	σ	-0.387	-0.397	$^1\Sigma_g^+$	-1.395	-1.407
$3s$	-0.222	-0.222	$^1S\ 1s3s$	-2.060	-2.061	σ	-0.243	-0.249			
$3p$	-0.221	-0.222									
$4s$	-0.125	-0.125	$^1S\ 2s^2$	-0.776	-0.778						
			$^1D\ 2p^2$	-0.674	-0.702						
			$^1P\ 2s2p$	-0.659	-0.693						
			$^1S\ 2p^2$	-0.599	-0.622						

FIG. 2. (Color online) Total single-electron capture cross sections as function of impact energy. Theory: present results (black solid line); Errea *et al.* [21] (note that the two sets of data with dash-dotted line in Fig. 1 of Ref. [21] have been merged for readability) (red dashed line); Kusakabe *et al.* [14] (blue dotted line); Shimakura *et al.* [22] (green dash-dotted line). Experiments: Okuno *et al.* [12] (red full circles); Figueira da Silva *et al.* [17] (black full squares); Kusakabe *et al.* [14] (black full triangles); Rudd *et al.* [7] (blue open circles); Shah and Gilbody [8] (green open squares).
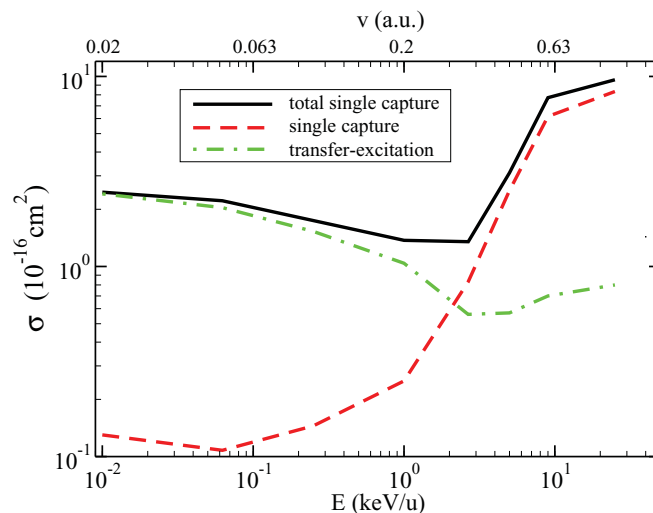

FIG. 3. (Color online) Cross sections for total single capture (solid line) and its two contributions, single capture (red dashed line) and transfer-excitation (green dot-dashed line) cross sections, as a function of impact energy and velocity.

transfer and transfer excitation, which leads systematically to dissociative transfer for an H_2 target [cf. Eq. (1)], are presented as function of impact energies. Our results, represented by the solid line, are compared with selected experimental and theoretical data that are representative of the general tendencies of the cross sections. As a common feature to the various sets of results, the cross sections for single-electron capture present a maximum at about 20 keV/u and decrease with impact energy down to 2 keV/u, where they exhibit a plateau-like structure down to about 100 eV/u. Then the experimental data show a further decrease while our results continue to present a rather flat behavior down to the lower energy that we considered, 10 eV/u. At that point we should stress again that our results are the only ones which extend over such a wide domain of energy (spreading on more than three decades), using the same semiclassical coupled-channel treatment (two active electrons, a complete molecular description of the target, same basis set): indeed the data of Errea *et al.* [21] are confined in the high energy domain and combine two models, MOCC with 2 electrons and for the highest energies 1-electron MOCC together with the independent particle model (IPM), the data of Shimakura *et al.* [22] extends on one decade of energy and steam from coupled channel calculations using a pseudo-molecular description of the target, finally the theoretical results presented in Ref. [14] stem from MOCC and only cover the low to intermediate energy range. Our results agree well with the available data but overestimate the extension of the plateau. The presence of this latter is characteristic of the competition between two mechanisms which dominate in distinct energy domains: at low energies and head-on collisions (see the discussion below) the dissociative electron transfer dominates but its contribution decreases steadily for increasing velocities while the pure single capture channel is a distant collision process (see below), leaving the ionized target H_2^+

in its ground state, and raises sharply to take over beyond about 2 keV/u ($v = 0.3$ a.u.; cf. Fig. 3). This behavior is in qualitative agreement with the related data presented in Errea *et al.* [21] and those obtained from the asymptotic model proposed by Khoma *et al.* [23]. Note however that these two treatments give an overestimation of the dissociative electron capture channels which explains that both sets of results lie at the upper limit of the experimental data while ours are at the lowest one.

As mentioned before the main disagreement between the experimental results reported in Refs. [12] and [17] and our results is related to the extension of the plateau structure down to 10 eV/u. This difference shows the limit of the rovibrational sudden approximation used in our calculations, cf. also [14]. At low collision energy the total single electron capture cross sections are dominated by the transfer-excitation (cf. Fig. 3 and [23]) which leads to the dissociation of the molecular target. At lowest energy (10 eV/u; i.e., an impact velocity of about 0.02 a.u.), the molecular dissociation takes place in the same time scale than the collision. Indeed in this energy domain the dissociation velocity is of the same order of magnitude than the collision velocity and the two target nuclei cannot be assumed fixed during the collision; the rovibrational sudden approximation breaks down and may give spurious results. The lower experimental values of single-electron-capture cross sections may then be due to the coupled dynamics of the two electrons in the field of the three moving nuclei which may favor orbiting, leading to the stabilization of He by double capture processes (cf. next section). According to Fig. 2, one may estimate the lower limit of validity of the rovibrational sudden approximation to about 0.1 keV/u.

The general discussion presented above concerning the dependencies of the cross sections is supported by the analysis of the transition probabilities of single-electron capture as function of impact parameter. In Fig. 4 we show the reduced probabilities for the dominant single-electron-capture channels at typical low ($v = 0.05$ a.u. or $E = 0.0625$ keV/u) and large ($v = 0.6$ a.u. or $E = 9$ keV/u) velocities. In the
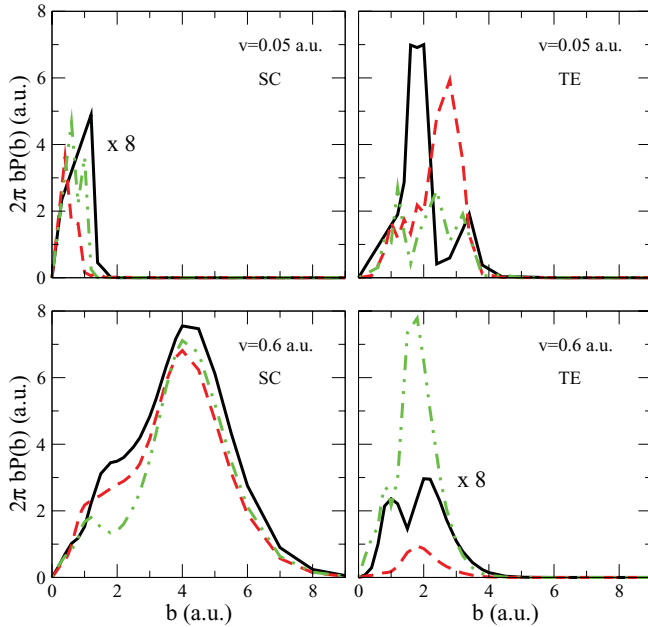
FIG. 4. (Color online) Transition probabilities for nondissociative (SC) and dissociative (TE) single-electron capture as a function of impact parameter for velocities 0.05 a.u. (top panels) and 0.6 a.u. (bottom panels) and three molecular orientations (Θ_m, Φ_m): (0,0) (green dash-dotted line), ($0, \frac{\pi}{2}$) (red dashed line), ($\frac{\pi}{2}, \frac{\pi}{2}$) (black solid line). Note that the main contributions for TE and SC channels are, respectively, H_2^{+*}-$He^+(1s)$ at low v and $He^+(2\ell)$ at high v.

former case, capture to the K shell of He^+, with simultaneous target excitation, is largely dominant while L-shell capture dominates the high-energy region, in agreement with the conclusions of previous works (e.g., [22] and [23]). Moreover, the figure shows that the single-electron-capture channel at low velocity is active for near head-on collisions ($b < 4$ a.u.) for which the orientation of the target with respect to the incoming projectile play a major role. In this range a very precise description of the transient three-center molecular structure which forms and evolutes during the scattering event should be considered. On the other hand, at high velocities the process is dominated by distant collisions (up to $b \approx 8$ a.u.) giving very similar behavior for the probabilities for the three considered orientations.

We turn now to the study of the double-capture channels, which strongly compete with the single-electron-capture channels at low energies.

C. Double-capture processes

Unlike single-electron capture, for which all available experimental results agree on the fact that the cross sections drop at collision energies below 0.1 keV/u, the behavior of double-electron-capture cross sections at low collision energy is still not well understood. Two tendencies are represented by both experimental and theoretical investigations: a fast and continuous increase for decreasing energies or a decrease below a few tens of eV/u. Figure 5 shows a series of representative results for double-capture processes in the energy domain ranging from 10 eV/u to 25 keV/u. The general behavior of the cross sections presents a V-valley shape with
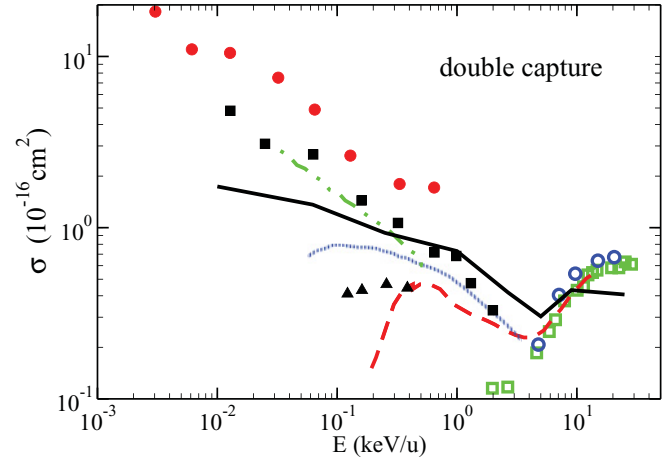

FIG. 5. (Color online) Double-electron-capture cross sections as function of impact energy. Theory: present results (black solid line); Errea *et al.* [21] (red dashed line); Kusakabe *et al.* [14] (blue dotted line); Shimakura *et al.* [22] (green dash-dotted line). Experiments: Okuno *et al.* [12] (red full circles); Figueira da Silva *et al.* [17] (black full squares); Kusakabe *et al.* [14] (black full triangles); Rudd *et al.* [7] (blue open circles); Shah and Gilbody [8] (green open squares).

a minimum at about 5 keV/u. If the various data, including ours, agree quite well for localizing the minimum and for the absolute values of the cross sections for the high-energy region, the results spread over one order of magnitude for low energies. The experimental data from Okuno *et al.* [12] (obtained by subtracting the single-capture cross sections from the attenuation ones) and from Figueira da Silva *et al.* [17] show a sharp increase for decreasing velocities—as a resonant process generally does—while those of Kusakabe *et al.* [14], confined to energies ranging from 100 to 500 eV/u, show a slow decrease. Theoretically, two sets of MOCC calculations [14,21] predict the latter behavior while the results of Shimakura *et al.* [22], although based on an approximate pseudo-molecular description of H_2, show an increase of the cross sections. Our results lie in the middle of these two extreme tendencies, showing an increase, although weaker than the experimental one. Comparing Figs. 2 and 5 in the low-energy region, our data show a nearly equivalent weight for single and double cross sections while Okuno *et al.* [12] and Figueira da Silva *et al.* [17] predict a strong (factor 10) dominance of double-electron capture over single-electron capture.

To get further insight into the mechanisms responsible of the double-electron capture channels, we show in Fig. 6 the related reduced transition probabilities as a function of the impact parameters for the same two characteristic collision energies (62.5 eV/u and 9 keV/u) and the three molecular orientations considered. Unlike single-electron capture, the same channels—double-electron capture to $He(1s2\ell)$—dominate the scattering for low and high energy with, in the latter case, a non-negligible contribution from the $He(1s^2)$ channel which takes over for energies above 20 keV/u. At high energy, the probabilities have a smooth shape indicating a complex coupled channel scheme, while for low energy they present sharp peaks which are characteristic of processes occurring at avoided crossings. This latter mechanism may explain the
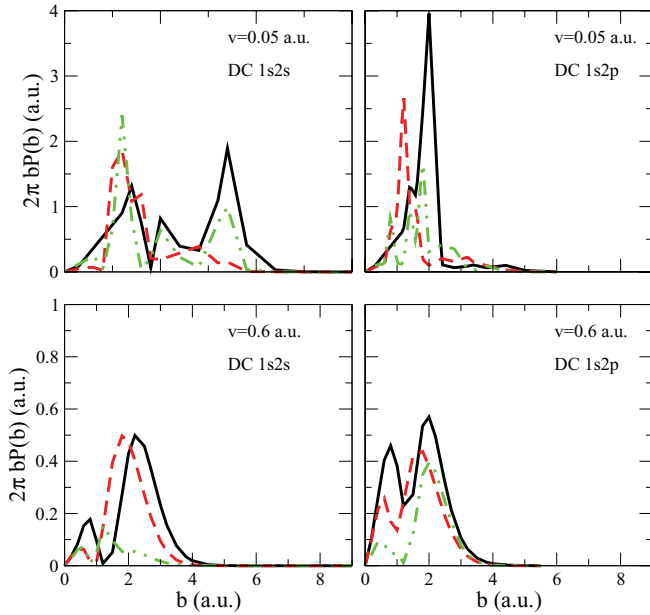
FIG. 6. (Color online) Transition probabilities for double-electron-capture into He($1s2\ell$) states as function of impact parameter for velocities 0.05 a.u. (top panels) and 0.6 a.u. (bottom panels) and for three molecular orientations (Θ_m, Φ_m): (0,0) (green dash-dotted line), $(0,\frac{\pi}{2})$ (red dashed line), $(\frac{\pi}{2},\frac{\pi}{2})$ (black solid line).

sharp increase of the cross sections for decreasing velocities and it is only the very accurate description of the three-center transient molecular structure which may produce ultimately converged cross sections in this energy range. It is therefore not surprising that our model, although highly refined but especially designed for intermediate velocities, cannot handle with optimal accuracy the description of such molecular mechanisms. It is worth noting, however, that the sum of our single-electron-capture and double-electron-capture cross sections for the lowest energies are close to the experimental sum, supporting the discussion above. The molecular description of the present approach (and calculations) may underestimate the probability of the transition of a second electron toward He$^+$ (leading to the neutralization of the projectile), in favor of a single excitation of H$_2{}^+$ (i.e., of transfer excitation) which is shown to be overestimated in Fig. 2. We should mention finally that this process, which is confined to near head-on collision trajectories (cf. Fig. 6), presents an important dependency on the molecular orientations. This could be probed in great detail by experiments involving multicoincidence measurements, as setups such as reaction microscopes [41] do.

Cross sections for double-electron capture into the lowest and most important doubly excited states of helium were also computed. Those excited states are metastable and decay by emitting an electron. The final states are then equivalent to direct single capture and ionization, also called transfer ionization. Therefore, in experimental investigations based on the detection of both ions of He, these processes contribute to the total single-electron capture. However, as will be shown below, the double electron capture channels into autoionizing states of helium are rather weak processes and can only modify experimental cross sections marginally, with no real implication for the discussion presented in
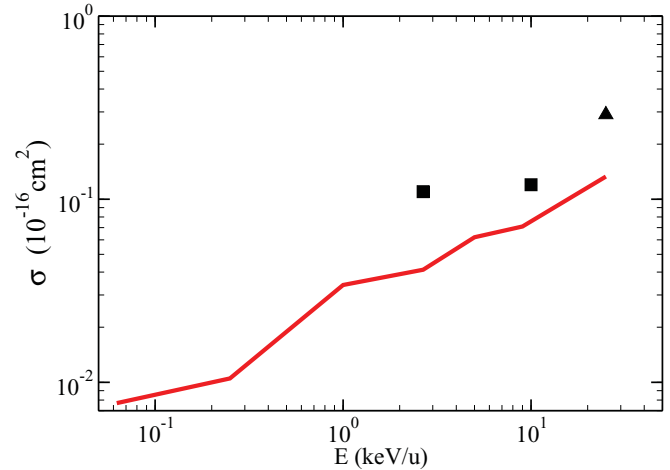

FIG. 7. (Color online) Cross sections for double-electron capture into doubly excited states of helium. Theory: present results (red solid line). Experiments: Frémont *et al.* [42] (squares) and Martinez *et al.* [16] (triangles).

the previous sections. The determination of converged cross sections for these weak channels is a delicate issue, both theoretically and experimentally; it thus represents a good test for our collision code. Moreover, the knowledge of these cross sections are required for the study of the feasibility at low energies of an interferometry experiment performed by Chesnel *et al.* [33,42] at high energy. Total cross sections for double electron capture into doubly excited states of helium are shown in Fig. 7, together with the only three available measurements from [16,42]. The computed cross sections are of the order of 10^{-17} cm^2 at 25 keV/u and decrease by a factor of about 10 from 25 keV/u to 100 eV/u impact energy. Note that their contribution to the total single-electron capture is about 10 times smaller than the direct double-electron capture processes. Considering the complexity of the calculations one may state that a good agreement is obtained between our data and the experimental ones. However, the decrease of the cross sections shown in our results do not support the weak dependency which can be extrapolated from the two lowest-energy experimental points. This tendency prevents the extension of the experimental investigation of Chesnel and collaborators to lower energies for the He^{2+}-H$_2$ collision system since cross sections of order of 10^{-18} cm^2 will require unreasonable detection times to be statistically relevant.

IV. CONCLUSIONS

In this paper we present a semiclassical close-coupling approach to simulate ion-molecule collisions involving two active electrons. This method is well adapted for keV/u collision energy but the extension of its use at much lower energies have been demonstrated. We have applied the method for the predictions of the total cross sections for single- and double-electron capture in He^{2+}-H$_2$ collisions for energies ranging from 10 eV/u to 25 keV/u. We have shown that the rovibrational sudden approximation used is valid for collision energies above about 100 eV/u for the system

considered. At lower collision energy, it overestimates the single-electron-capture cross sections and more extensive basis-set calculations or a converged three-center MOCC approach are required. Cross sections for double-electron capture into bound states and autoionizing states of helium have been shown and compared to the available experimental and theoretical data. Good agreement with the most recent results have been achieved. The results reported in the article show that the present method is a powerful tool to study one- and two-electron processes in ion-molecule keV collisions. The extension of the present method and computer codes to polyatomic and polyelectronic molecular targets is straightforward, although very demanding in computer resources, memory, and CPU time. We are presently planning this development, taking into account the electronic correlation and the multicenter character of the target, in order to pave the way to go beyond the effective single-center-target approximations in quantal calculations (cf. e.g., [47]) or classical independent-electron treatments [48] used to describe ion-H_2O collisions.

APPENDIX A: METHOD AND STRATEGY FOR COMPUTATIONS OF DIFFERENT COUPLING MATRIX ELEMENTS

To develop the new computer code we based the representation of the scattering state on a Gaussian-type orbital (GTOs) basis set which allow the analytical expression of the required matrix elements of $\underline{\underline{M}}$ and $\underline{\underline{S}}$ [see Eq. (7)] and, therefore, a considerable speedup of the calculations over Slater-type orbital (STOs) expansions. Procedures for the evaluation of one-electron and two-electron two-center integrals have been presented respectively in Caillat *et al.* [30] and Wang *et al.* [43] (and references therein). We report here a modified version of the method which allows us to evaluate two-electron three-center integrals. To build a completely general procedure we based the computations of those matrix elements on symbolic derivations of genuine integrals. We present in the following the formalism for multicenter one-electron integrals, two-center two-electron integrals extended to three-center two-electron integrals by using well-known translation properties of GTOs.

1. One-electron integrals computations

Multicenter one-electron integrals can be written in a general form as

$$I = \int_0^\infty dx \int_0^\infty dy \int_0^\infty dz\, r^{m_1} r'^{m_2} r''^{m_3} x^{u_1} y^{v_1} z^{w_1} x'^{u_2} y'^{v_2} z'^{w_2}$$
$$\times \frac{\exp\left(-\alpha_1 r^2 - \alpha_2 r'^2 - \alpha_3 r''^2 + i\mu\vec{v}\cdot\vec{r}\right)}{(r'')^\lambda} \quad (\lambda = 0,1;\ \mu = 0, \pm 1), \tag{A1}$$

where $u_1, v_1, \ldots, w_2, m_1, m_2$, and m_3 are positive integers or zero. Vectors $\vec{r}$, $\vec{r}'$, and $\vec{r}''$ are the electron coordinates with respect to the origin, the projectile and potential center ($\vec{r}' = \vec{r} - \vec{R}$ and $\vec{r}'' = \vec{r} - \vec{\rho}$), respectively. This general form allows us to define all kind of useful integrals, with potential ($\lambda = 1$) or without ($\lambda = 0$, $\alpha_3 = 0$), with ETF ($\mu = 1$) or without ($\mu = 0$), as well as for two centers ($\vec{\rho} = \vec{R}$ or $\vec{0}$) or three. The integral I is written as derivatives of the genuine integral J_λ as

$$I = \lim_{\vec{a}\to\mu\vec{v}} \lim_{\vec{b}\to\vec{0}} \left(-i\frac{\partial}{\partial a_x}\right)^{u_1} \left(-i\frac{\partial}{\partial a_y}\right)^{v_1} \left(-i\frac{\partial}{\partial a_z}\right)^{w_1} \left(-i\frac{\partial}{\partial b_x}\right)^{u_2} \left(-i\frac{\partial}{\partial b_y}\right)^{v_2} \left(-i\frac{\partial}{\partial b_z}\right)^{w_2}$$
$$\times \left(-i\frac{\partial}{\partial \alpha_1}\right)^{\frac{m_1}{2}} \left(-i\frac{\partial}{\partial \alpha_2}\right)^{\frac{m_2}{2}} \left(-i\frac{\partial}{\partial \alpha_3}\right)^{\frac{m_3}{2}} J_\lambda, \tag{A2}$$

where J_λ is

$$J_\lambda = \int_0^\infty dx \int_0^\infty dy \int_0^\infty dz \frac{\exp\left(-\alpha_1 r^2 - \alpha_2 r'^2 - \alpha_3 r''^2 + i\vec{a}\cdot\vec{r} + i\vec{b}\cdot\vec{r}'\right)}{(r'')^\lambda} \quad (\lambda = 0,1). \tag{A3}$$

and the powers m_1, m_2, and m_3 must be even. The analytical form of J_λ can be expressed as

$$J_1 = \frac{2\pi^{3/2}}{B\sqrt{\alpha}} \exp\left(-\alpha_2 R^2 - \alpha_3 \rho^2 - i\vec{b}\cdot\vec{R}\right) e^{A^2/(4\alpha)} \text{erf}\left(\frac{B}{2\sqrt{\alpha}}\right), \tag{A4}$$

for integrals with potential ($\lambda = 1$) and

$$J_0 = \left(\frac{\pi}{\alpha}\right)^{3/2} \exp\left(-\alpha_2 R^2 - i\vec{b}\cdot\vec{R}\right) e^{A^2/(4\alpha)}, \tag{A5}$$

for integrals without potential ($\lambda = 0$), where the various parameters used above are defined as

$$\alpha = \alpha_1 + \alpha_2 + \alpha_3, \quad \vec{A} = i\vec{a} + 2\alpha_2\vec{R} + 2\alpha_3\vec{\rho}, \quad \vec{B} = \vec{A} - 2\alpha\vec{\rho}. \tag{A6}$$

The derivatives defined in Eq. (A3) are then done symbolically directly in the FORTRAN computer code and then evaluated numerically. Two-electron integrals are computed using the same strategy. However, more derivatives have to be performed as presented in the following.

2. Two-electron two-center integrals computations

Four types of two-electron two-center integrals have to be computed, namely, E, D, E', and E'', which are defined as

$$E = \int\int d\vec{r}_1 d\vec{r}_2 G^*_{\alpha_a,l_a,m_a}(\vec{r}_1) G^*_{\alpha_b,l_b,m_b}(\vec{r}_2^P) \frac{e^{i\vec{v}\cdot(\vec{r}_1-\vec{r}_2)}}{|\vec{r}_1-\vec{r}_2|} G_{\alpha_c,l_c,m_c}(\vec{r}_1^P) G_{\alpha_d,l_d,m_d}(\vec{r}_2), \tag{A7}$$

$$D = \int\int d\vec{r}_1 d\vec{r}_2 G^*_{\alpha_a,l_a,m_a}(\vec{r}_1) G^*_{\alpha_b,l_b,m_b}(\vec{r}_2^P) \frac{1}{|\vec{r}_1-\vec{r}_2|} G_{\alpha_c,l_c,m_c}(\vec{r}_1) G_{\alpha_d,l_d,m_d}(\vec{r}_2^P), \tag{A8}$$

$$E' = \int\int d\vec{r}_1 d\vec{r}_2 G^*_{\alpha_a,l_a,m_a}(\vec{r}_1) G^*_{\alpha_b,l_b,m_b}(\vec{r}_2^P) \frac{e^{-i\vec{v}\cdot(\vec{r}_2)}}{|\vec{r}_1-\vec{r}_2|} G_{\alpha_c,l_c,m_c}(\vec{r}_1) G_{\alpha_d,l_d,m_d}(\vec{r}_2), \tag{A9}$$

$$E'' = \int\int d\vec{r}_1 d\vec{r}_2 G^*_{\alpha_a,l_a,m_a}(\vec{r}_1) G^*_{\alpha_b,l_b,m_b}(\vec{r}_2) \frac{e^{i\vec{v}\cdot(\vec{r}_1+\vec{r}_2)}}{|\vec{r}_1-\vec{r}_2|} G_{\alpha_c,l_c,m_c}(\vec{r}_1^P) G_{\alpha_d,l_d,m_d}(\vec{r}_2^P), \tag{A10}$$

where $\vec{r}_i^P = \vec{r}_i - \vec{R}$ is the position vector of electron i with respect to the projectile. As for the one-electron integrals, the four kinds of two-electron, two-center integrals are defined in Cartesian coordinates. For instance, E is written as

$$\tilde{E} = \int\int d\vec{r}_1 d\vec{r}_2 r_1^{n_a} e^{-\alpha_a r_1^2} x_1^{u_a} y_1^{v_a} z_1^{w_a} r_2'^{n_b} e^{-\alpha_b r_2'^2} x_2'^{u_b} y_2'^{v_b} z_2'^{w_b} \frac{e^{i\vec{v}\cdot(\vec{r}_1+\vec{r}_2)}}{|\vec{r}_1-\vec{r}_2|} r_1'^{n_c} e^{-\alpha_c r_1'^2} x_1'^{u_c} y_1'^{v_c} z_1'^{w_c} r_2^{n_d} e^{-\alpha_d r_2^2} x_2^{u_d} y_2^{v_d} z_2^{w_d}, \tag{A11}$$

where we try to keep the n_i ($i = a$, b, c, or d) equal to zero in order to have less computational efforts without loss of generality. Integrals $\tilde{D}$, $\tilde{E}'$, $\tilde{E}''$ are defined the same way and are all evaluated by derivations of the genuine integral I as

$$I(\alpha_a,\alpha_b,\alpha_c,\alpha_d) = \int\int d\vec{r}_1 d\vec{r}_2 e^{-\alpha_a r_1^2 - \alpha_b r_2'^2 - \alpha_c r_1'^2 - \alpha_d r_2^2} \frac{e^{i\vec{v}\cdot(\vec{r}_1+\vec{r}_2)}}{|\vec{r}_1-\vec{r}_2|} \exp(i\vec{a}\cdot\vec{r}_1 + i\vec{b}\cdot\vec{r}_2' + i\vec{c}\cdot\vec{r}_1' + i\vec{d}\cdot\vec{r}_2), \tag{A12}$$

with, for example for $\tilde{E}$,

$$\tilde{E} = \lim_{\vec{a},\vec{b},\vec{c},\vec{d}\to\vec{0}} \left(-i\frac{\partial}{\partial a_x}\right)^{u_a} \left(-i\frac{\partial}{\partial a_y}\right)^{v_a} \left(-i\frac{\partial}{\partial a_z}\right)^{w_a} \left(-i\frac{\partial}{\partial b_x}\right)^{u_b}$$
$$\cdots \left(-i\frac{\partial}{\partial d_z}\right)^{w_d} \left(-i\frac{\partial}{\partial \alpha_a}\right)^{\frac{n_a}{2}} \left(-i\frac{\partial}{\partial \alpha_b}\right)^{\frac{n_b}{2}} \left(-i\frac{\partial}{\partial \alpha_c}\right)^{\frac{n_c}{2}} \left(-i\frac{\partial}{\partial \alpha_d}\right)^{\frac{n_d}{2}} I(\alpha_a,\alpha_b,\alpha_c,\alpha_d). \tag{A13}$$

Integral I is obtained analytically

$$I(\alpha_a,\alpha_b,\alpha_c,\alpha_d) = \frac{\pi^{5/2}}{\alpha^{1/2}} \frac{\exp[-(\alpha_c+\alpha_b)R^2 - i(\vec{b}+\vec{c})\vec{R}]}{\alpha_{ac}^{3/2}\alpha_{bd}^{3/2}} \exp\left(\frac{B^2}{4\alpha_{ac}} + \frac{D^2}{4\alpha_{bd}}\right) M\left(\frac{1}{2};\frac{3}{2};-\frac{\beta^2}{\alpha}\right), \tag{A14}$$

with

$$\alpha_{ac} = \alpha_a + \alpha_c, \quad \alpha_{bd} = \alpha_b + \alpha_d, \quad \alpha = \frac{1}{4\alpha_{ac}} + \frac{1}{4\alpha_{bd}}, \quad B^2 = B_x^2 + B_y^2 + B_z^2, \quad B_i = 2\alpha_c R_i + i(a_i + c_i + v_i),$$

$$D^2 = D_x^2 + D_y^2 + D_z^2, \quad D_i = 2\alpha_b R_i + i(b_i + d_i - v_i), \quad \beta^2 = \beta_x^2 + \beta_y^2 + \beta_z^2, \quad \beta_i = \frac{B_i}{4\alpha_{ac}} + \frac{D_i}{4\alpha_{bd}},$$

and $M(a,b,z)$ are the confluent hypergeometric functions. Integrals D, E', and E'' are computed the same way but the derivatives and the limits of the parameters are different.

3. Two-electron three-center integrals computations

For the treatment of ion-diatomic molecule collisions with the close-coupling method, two-electron three-center integrals have to be computed. To do so we use the properties of the GTOs and methods similar to those presented above.

The product of two GTOs G_1 and G_2 centered respectively on A and B:

$$G_1 = x_A^{l_1} y_A^{m_1} z_A^{n_1} e^{-\alpha_1 r_A^2}, \tag{A15}$$

$$G_2 = x_B^{l_2} y_B^{m_2} z_B^{n_2} e^{-\alpha_2 r_B^2}, \tag{A16}$$

can be written as a third Gaussian G_3 centered on a third point P:

$$G_3 = G_1 G_2 = x_A^{l_1} x_B^{l_2} y_A^{m_1} y_B^{m_2} z_A^{n_1} z_B^{n_2}$$
$$\times \exp(-\alpha_1\alpha_2 AB^2/\gamma)\exp\left(-\gamma r_P^2\right), \tag{A17}$$

with

$$\gamma = \alpha_1 + \alpha_2, \quad \vec{r}_P = \frac{\alpha_1\vec{r}_A + \alpha_2\vec{r}_B}{\gamma}.$$

Moreover, $x_A^{l_1} x_B^{l_2}$ can be written as

$$x_A^{l_1} x_B^{l_2} = \sum_{k=0}^{l_1+l_2} x_p^k f_k(l_1, l_2, (\overline{\mathbf{PA}})_x, (\overline{\mathbf{PB}})_x), \qquad (A18)$$

with

$$\begin{aligned} & f_k(l_1, l_2, (\overline{\mathbf{PA}})_x, (\overline{\mathbf{PB}})_x) \\ & = \sum_{i=0,l_1}^{i+j=k} \sum_{j=0,l_2} (\overline{\mathbf{PA}})_x^{l_1-i} C_i^{l_1} (\overline{\mathbf{PB}})_x^{l_2-j} C_j^{l_2}. \end{aligned} \qquad (A19)$$

For an easier implementation in the code, the f_k coefficients can be written as

$$\begin{aligned} f_k &= \sum_{q=\max(-k,k-2l_2)}^{\min(k,2l_1-k)} C_i^{l_1} C_j^{l_2} (\overline{\mathbf{PA}})_x^{l_1-i} (\overline{\mathbf{PB}})_x^{l_2-j}, \\ & 2i = k+q, \quad 2j = k-q \end{aligned} \qquad (A20)$$

where q increases by step of two.

There are 36 kinds of two-electron three-center integrals which can be sorted into the four types of two-electron, two-center integrals presented before:

(i) of type E: $\langle AP||PB \rangle$, $\langle BP||PA \rangle$, $\langle PA||BP \rangle$, and $\langle PB||AP \rangle$,

(ii) of type D: $\langle AP||BP \rangle$, $\langle BP||AP \rangle$, $\langle PA||PB \rangle$, and $\langle PB||PA \rangle$,

(iii) of type E': $\langle AA||BP \rangle$, $\langle AB||AP \rangle$, $\langle AB||BP \rangle$, $\langle AB||PA \rangle$, $\langle AB||BP \rangle$, $\langle AP||AB \rangle$, $\langle AP||BA \rangle$, $\langle AP||BB \rangle$, $\langle BA||AP \rangle$, $\langle BA||BP \rangle$, $\langle BA||PA \rangle$, $\langle BA||PB \rangle$, $\langle BP||AA \rangle$, $\langle BP||AB \rangle$, $\langle BP||BA \rangle$, $\langle PA||AB \rangle$, $\langle PA||BA \rangle$, $\langle PA||BB \rangle$, $\langle PB||AA \rangle$, $\langle PB||AB \rangle$, $\langle PB||BA \rangle$, $\langle AA||PB \rangle$, $\langle BB||AP \rangle$ and $\langle BB||PA \rangle$,

(iv) of type E'': $<\langle AB||PP \rangle$, $\langle BA||PP \rangle$, $\langle PP||AB \rangle$ and $\langle PP||BA \rangle$,

where, for simplicity, we note the states Φ^I ($I = A$, B, P) by the corresponding letter and A, B, P correspond to the two centers of the molecular target and the projectile, respectively. The bracket notation used is defined such as; for example, the integrals $\langle AB||PP \rangle$ of type E'' is given by

$$\langle AB||PP \rangle = \int d\vec{r}_1 \int d\vec{r}_2 x_{A1}^{u_a} y_{A1}^{v_a} z_{A1}^{w_a} e^{-\alpha_a r_{A1}^2} x_{B2}^{u_b} y_{B2}^{v_b} z_{B2}^{w_b} e^{-\alpha_b r_{B2}^2} \frac{e^{i\vec{v}\cdot(\vec{r}_1+\vec{r}_2)}}{|r_{12}|} x_{P1}^{u_c} y_{P1}^{v_c} z_{P1}^{w_c} e^{-\alpha_c r_{P1}^2} x_{P2}^{u_d} y_{P2}^{v_d} z_{P2}^{w_d} e^{-\alpha_d r_{P2}^2}, \qquad (A21)$$

which can be written as

$$\begin{aligned} \langle AB||PP \rangle &= \int d\vec{r}_1 \int d\vec{r}_2 \sum_{k=0}^{u_a+u_c} \sum_{l=0}^{v_a+v_c} \sum_{m=0}^{w_a+w_c} f_k x_{S1}^k e_l y_{S1}^l g_m z_{S1}^m K e^{-\gamma r_{S1}^2} \frac{e^{i\vec{v}(\vec{r}_1+\vec{r}_2)}}{|r_{12}|} \sum_{n=0}^{u_b+u_d} \sum_{o=0}^{v_b+v_d} \sum_{p=0}^{w_b+w_d} h_n x_{T2}^n i_o y_{T2}^o j_p z_{T2}^p L e^{-\omega r_{T2}^2} \\ &= \sum_{k=0}^{u_a+u_c} \sum_{l=0}^{v_a+v_c} \sum_{m=0}^{w_a+w_c} \sum_{n=0}^{u_b+u_d} \sum_{o=0}^{v_b+v_d} \sum_{p=0}^{w_b+w_d} f_k e_l g_m h_n i_o j_p I, \end{aligned} \qquad (A22)$$

with

$$\gamma = \alpha_a + \alpha_c, \quad \omega = \alpha_b + \alpha_d, \quad K = e^{-\alpha_a \alpha_c (\overline{AP})/\gamma}, \quad L = e^{-\alpha_b \alpha_d (\overline{BP})/\omega}, \qquad (A23)$$

$$\vec{R}_S = \frac{\alpha_a \vec{R}_A + \alpha_c \vec{R}_P}{\gamma}, \quad \vec{R}_T = \frac{\alpha_b \vec{R}_B + \alpha_d \vec{R}_P}{\omega}. \qquad (A24)$$

The coefficients $(f_k, e_l, \dots,)$ in Eq. (A22) are given by the generic formula in Eq. (A20) and the integral I is expressed as

$$I = \int d\vec{r}_1 \int d\vec{r}_2 x_{S1}^k y_{S1}^l z_{S1}^m K e^{-\gamma r_{S1}^2} \frac{e^{i\vec{v}\cdot(\vec{r}_1+\vec{r}_2)}}{|r_{12}|} x_{T2}^n y_{T2}^o z_{T2}^p L e^{-\omega r_{T2}^2}, \qquad (A25)$$

with $\vec{r}_{Si} = \vec{r}_i - \vec{R}_S$ and $\vec{r}_{Ti} = \vec{r}_i - \vec{R}_T$. Finally, the integral I is rewritten as

$$I = K L e^{2i\vec{v}\cdot\vec{R}_S} I', \qquad (A26)$$

where K and L are defined in Eq. (A23) and with the integral I' defined as

$$I' = \int d\vec{r}_1 \int d\vec{r}_2 x_{S1}^k y_{S1}^l z_{S1}^m e^{-\gamma r_{S1}^2} \frac{e^{i\vec{v}\cdot(\vec{r}_{S1}+\vec{r}_{S2})}}{|r_{12}|} x_{T2}^n y_{T2}^o z_{T2}^p e^{-\omega r_{T2}^2}. \qquad (A27)$$

The integral I' is then computed as E'' [cf. Eq. (A10)].

TABLE II. Parameters of the 17 (+10 when taking into account the m quantum numbers) GTOs used to describe states of He$^+$ and He.

i	ℓ	α_i	i	ℓ	α_i	i	ℓ	α_i	i	ℓ	α_i	i	ℓ	α_i
1	0	0.007 89	5	0	0.156 60	9	0	8.891 43	13	1	0.031 59	17	1	1.212 18
2	0	0.025 74	6	0	0.231 60	10	0	17.097 29	14	1	0.112 96			
3	0	0.097 86	7	0	0.899 67	11	0	28.517 21	15	1	0.230 68			
4	0	0.128 37	8	0	2.722 46	12	0	75.299 00	16	1	0.295 76			

APPENDIX B: OPTIMIZED GAUSSIAN-TYPE ORBITALS FOR He^{2+}-H$_2$ COLLISIONS

The atomic and molecular states used in the present work were obtained by diagonalization of the electronic Hamiltonian onto basis sets composed of Gaussian-type orbitals (GTO)s. These latter are defined as

$$G_{\alpha_i,\ell,m}(\vec{r}) = Y_{\ell,m}(\hat{\mathbf{r}})r^\ell e^{-\alpha_i r^2}, \tag{B1}$$

with the exponents α_i of the GTOs optimized by a genetic algorithm in order to accurately describe the one- and two-electron bound states of the isolated collision partners. The

TABLE III. Parameters of the 7 GTOs centered on each nucleus used to describe states of H$_2^+$ and H$_2$.

i	ℓ	α_i	i	ℓ	α_i
1	0	0.020 64	5	0	0.796 66
2	0	0.118 73	6	0	4.019 96
3	0	0.174 13	7	0	25.764 3
4	0	0.238 97			

optimized parameters for (He$^+$, He) and (H$_2^+$, H$_2$) used in the present calculations are listed in Tables II and III, respectively.

[1] T. E. Cravens, Science **296**, 1042 (2002).

[2] R. K. Janev, Contemp. Phys. **46**, 121 (2005).

[3] U. Amaldi and G. Kraft, Rep. Prog. Phys. **68**, 1861 (2005).

[4] Dz. Belkić, J. Math. Chem. **47**, 1366 (2010).

[5] J. Caillat, N. Sisourat, A. Dubois, I. Sundvor, and J. P. Hansen, Phys. Rev. A **73**, 014701 (2006).

[6] P. Hvelplund and A. Andersen, Phys. Scr. **26**, 375 (1982).

[7] M. E. Rudd, T. V. Goffe, and A. Itoh, Phys. Rev. A **32**, 2128 (1985).

[8] M. B. Shah and H. B. Gilbody, J. Phys. B **7**, 256 (1974).

[9] M. B. Shah and H. B. Gilbody, J. Phys. B **9**, 1933 (1976).

[10] G. J. Frieling *et al.*, J. Phys. B **25**, 1245 (1992).

[11] M. B. Shah, P. McCallion, and H. B. Gilbody, J. Phys. B **22**, 3983 (1989).

[12] K. Okuno, K. Soejima, and Y. Kaneko, J. Phys. B **25**, L105 (1992).

[13] T. Kusakabe, H. Yoneda, Y. Mizumoto, and K. Katsurayama, J. Phys. Soc. Jpn. **59**, 1218 (1990).

[14] T. Kusakabe, Y. Miyamoto, M. Kimura, and H. Tawara, Phys. Rev. A **73**, 022706 (2006).

[15] S. Martínez, G. Bernardi, P. Focke, D. Fregenal, and S. Suárez, Phys. Rev. A **72**, 062722 (2005).

[16] S. Martínez, G. Bernardi, P. Focke, A. D. González, and S. Suárez, J. Phys. B **35**, 2261 (2002).

[17] S. Figueira da Silva, H. P. Winter, and F. Aumayr, Phys. Rev. A **75**, 042706 (2007).

[18] M. E. Galassi, R. D. Rivarola, and P. D. Fainstein, Phys. Rev. A **70**, 032721 (2004).

[19] J. B. Delos, Rev. Mod. Phys. **53**, 287 (1981).

[20] L. F. Errea, J. D. Gorfinkiel, A. Macías, L. Méndez, B. Pons, and A. Riera, J. Phys. B **30**, 3855 (1997).

[21] L. F. Errea, A. Macias, L. Méndez, B. Pons, and A. Riera, J. Phys. B **36**, L135 (2003).

[22] N. Shimakura, M. Kimura, and N. F. Lane, Phys. Rev. A **47**, 709 (1993).

[23] M. V. Khoma, V. Y. Lazur, and R. K. Janev, Phys. Rev. A **80**, 032706 (2009).

[24] B. H. Bransden and M. R. C. McDowell, *Charge Exchange and the Theory of Ion-Atom Collisions* (Oxford University Press, New York, USA, 1992).

[25] W. Fritsch, Phys. Rev. A **46**, 3910 (1992).

[26] H. J. Lüdde, T. Spranger, M. Horbatsch, and T. Kirchner, Phys. Rev. A **80**, 060702(R) (2009).

[27] A. Dubois *et al.*, Nucl. Instrum. Meth. B **241**, 48 (2005).

[28] C. Illescas and A. Riera, Phys. Rev. A **60**, 4546 (1999).

[29] K. V. Cornelius, Phys. Rev. A **73**, 032710 (2006).

[30] J. Caillat, A. Dubois, I. Sundvor, and J. P. Hansen, Phys. Rev. A **70**, 032715 (2004).

[31] F. Martín and A. Salin, Phys. Rev. A **54**, 3990 (1996).

[32] R. O. Barrachina and M. Zitnik, J. Phys. B **37**, 3847 (2007).

[33] J-Y. Chesnel, A. Hajaji, R. O. Barrachina, and F. Frémont, Phys. Rev. Lett. **98**, 100403 (2007).

[34] W. Fritsch and C. D. Lin, Phys. Rep. **202**, 1 (1991).

[35] This specific choice of ETFs is only related to the schematic representation of the collision system given in Fig. 1, where the center of mass of the molecular target defines the origin of the reference frame. This is done only for convenience and the results do not depend on this specific choice.

[36] L. F. Shampine and M. K. Gordon, in *Computer Solution of Ordinary Differential Equations: the Initial Value Problem* (Freeman, San Fransisco, 1975).

[37] J. M. Hodgkinson, T. K. McLaughlin, R. W. McCullough, J. Geddes, and H. B. Gilbody, J. Phys. B **28**, L393 (1995).

[38] R. Hoekstra, H. O. Folkerts, J. P. M. Beijers, R. Morgenstern, and F. J. de Heer, J. Phys. B **27**, 2021 (1994).

[39] L. F. Errea, A. Macías, L. Méndez, B. Pons, and A. Riera, J. Chem. Phys. **119**, 325 (2003).

[40] V. V. Afrosimov, G. A. Leiko, and M. N. Panov, Zh. Tekh. Fiz. **50**, 519 (1980) [Sov. Phys. Tech. Phys. **25**, 313 (1980)].

[41] R. Dörner, V. Mergel, O. Jagutzki, L. Spielberger, J. Ullrich, R. Moshammer, and H. Schmidt-Böcking, Physics Report **330**, 95 (2000).

[42] F. Frémont, S. Suarez, R. O. Barrachina, A. Hajaji, N. Sisourat, A. Dubois, and J.-Y. Chesnel, Nucl. Instrum. Methods Phys. Res., Sect. B **267**, 206 (2009).

[43] J. Wang, J. P. Hansen, and A. Dubois, J. Phys. B **33**, 241 (2000).

[44] Y. Ralchenko, A. E. Kramida, J. Reader, and NIST ASD Team. NIST Atomic Spectra Database, National Institute of Standards and Technology, Gaithersburg, Maryland, USA. Available at [http://physics.nist.gov/asd3] (2011).

[45] K. Iemura *et al.*, Phys. Rev. A **64**, 062709 (2001).

[46] T. E. Sharp, Atom. Data **2**, 119 (1971).

[47] C. Champion, O. Boudrioua, and C. Dal Cappello, J. Phys. Conf. Ser. **101**, 012010 (2008).

[48] C. Illescas, L. F. Errea, L. Méndez, B. Pons, I. Rabadán, and A. Riera, Phys. Rev. A **83**, 052704 (2011).